

## Journal Pre-proof

Irrigation cooling effect on land surface temperature across China based on satellite observations

Qiquan Yang, Xin Huang, Qihong Tang



PII: S0048-9697(19)35979-0

DOI: <https://doi.org/10.1016/j.scitotenv.2019.135984>

Reference: STOTEN 135984

To appear in: *Science of the Total Environment*

Received date: 9 October 2019

Revised date: 5 December 2019

Accepted date: 5 December 2019

Please cite this article as: Q. Yang, X. Huang and Q. Tang, Irrigation cooling effect on land surface temperature across China based on satellite observations, *Science of the Total Environment* (2019), <https://doi.org/10.1016/j.scitotenv.2019.135984>

This is a PDF file of an article that has undergone enhancements after acceptance, such as the addition of a cover page and metadata, and formatting for readability, but it is not yet the definitive version of record. This version will undergo additional copyediting, typesetting and review before it is published in its final form, but we are providing this version to give early visibility of the article. Please note that, during the production process, errors may be discovered which could affect the content, and all legal disclaimers that apply to the journal pertain.

© 2019 Published by Elsevier.

## **Irrigation cooling effect on land surface temperature across China based on satellite observations**

Qiquan Yang <sup>a</sup>, Xin Huang <sup>a, b, \*</sup>, Qihong Tang <sup>c, d, \*</sup>

<sup>a</sup> School of Remote Sensing and Information Engineering, Wuhan University, Wuhan, 430079, P.R. China.

<sup>b</sup> State Key Laboratory of Information Engineering in Surveying, Mapping and Remote Sensing, Wuhan University, Wuhan, 430079, P.R. China.

<sup>c</sup> Key Laboratory of Water Cycle and Related Land Surface Processes, Institute of Geographic Sciences and Natural Resources Research, Chinese Academy of Sciences, Beijing, 100101, P.R. China.

<sup>d</sup> College of Resources and Environment, University of Chinese Academy of Sciences, Beijing 100049, P.R. China.

\* Corresponding author. Email: tangqh@igsrr.ac.cn (Q. Tang), xhuang@whu.edu.cn (X. Huang)

### **Abstract**

The effect of irrigation on temperature has attracted much attention because its cooling effect may mask the warming due to other factors, such as greenhouse gas forcing. Although many studies have examined the irrigation cooling effect (ICE) based on near-surface air temperature from meteorological observations or climate model simulations, few

studies have directly addressed the effect of irrigation on land surface temperature (LST), which is closely linked to the surface energy balance and near-surface air temperature. In this paper, an ICE detection (ICED) method is proposed to assess the effect of irrigation on LST using the Moderate Resolution Imaging Spectroradiometer (MODIS) products across China. The magnitude of the ICE is calculated as the LST difference between irrigated area and adjacent non-irrigated area in the self-adaptive moving window determined by the ICED method. The results show that irrigation cools daytime LST by 1.15 K, and cools nighttime LST by 0.13 K, on average, across irrigated areas in China. The effect of irrigation on LST differs greatly among the climate zones and seasons, characterized by the enhanced ICE in arid regions and the growing season. In the arid climate zone, nearly all the irrigated areas show a lower daytime LST than the adjacent non-irrigated areas, leading to a strong ICE magnitude of greater than 6 K in the growing season. In the humid climate zone, the impact of irrigation on LST is generally negligible, with a magnitude around zero throughout the year. This study provides observational evidence and a comprehensive assessment of the effect of irrigation on LST. The proposed ICED method has the potential to be used to study the spatiotemporal variation of the effect of irrigation on LST over other regions with intensive irrigation.

*Keywords:* irrigated area, remote sensing, observational evidence,

spatiotemporal variations, Google Earth Engine

## 1. Introduction

The accelerating anthropogenic activities have had significant influence on the Earth's surface properties, by either altering land surface properties or modifying the characteristics of the existing land cover (Goonetilleke et al., 2005; Grimm et al., 2008; Thiery et al., 2017). Irrigation is one of the most pervasive land management activities (Sacks et al., 2009), and contributes greatly to global food production (Godfray et al., 2010; Ozdogan, 2011). Irrigation can enhance soil moisture, increase evapotranspiration, and change land surface properties (Seneviratne et al., 2010; Thiery et al., 2017). These biophysical impacts of irrigation affect the energy budget, resulting in feedback to the local climate, and have potential cooling effect on temperature (Biggs et al., 2008; Kang and Eltahir, 2019; Nocco et al., 2019; Thiery et al., 2017; Wen and Jin, 2012; Zhang et al., 2017).

The effect of irrigation on near-surface air temperature has been investigated in numerous studies, using climate models (Broadbent et al., 2018; Chen and Jeong, 2018; Chou et al., 2018; de Vrese and Hagemann, 2017; Lobell et al., 2009; Lobell et al., 2008b; Sacks et al., 2009; Wu et al., 2018; Zhang et al., 2017) and/or the analysis of meteorological observations (Bonfils and Lobell, 2007; Chen et al., 2018; Han and Yang,

2013; Lobell and Bonfils, 2008; Lobell et al., 2008a; Mahmood et al., 2006; Nocco et al., 2019; Roy et al., 2007; Shi et al., 2014). Most of these studies have indicated the irrigation cooling effect (ICE) on near-surface air temperature. For example, by the use of a modeling methods, Zhang et al. (2017) revealed that irrigation decreased mean air temperature by about 1.7 K over a river basin located in Northwest China; and Broadbent et al. (2018) found that irrigation reduced diurnal average air temperature by 2.3 K in an urban area of Australia. Furthermore, an obvious ICE has been reported in several observational studies based on meteorological stations located in irrigated areas of China (Han and Yang, 2013; Shi et al., 2014), America (Bonfils and Lobell, 2007; Chen et al., 2018; Lobell and Bonfils, 2008; Nocco et al., 2019), and other countries (Lobell et al., 2008a; Roy et al., 2007). However, these studies, both modeling and observational, have mostly focused on near-surface air temperature, and few have analyzed the effect of irrigation on land surface temperature (LST) which is recognized as being one of the most important climate and environmental indices (King, 1999; Wan et al., 2010). Although correlated with air temperature, LST differs from it in physical meaning, magnitude, and influencing factors (Jin and Dickinson, 2010; Mildrexler et al., 2011; Shiflett et al., 2017). Air temperature is largely dependent on the atmospheric conditions, whereas LST is in addition significantly influenced by soil moisture, land surface properties, and surface energy

fluxes (e.g. latent heat and sensible heat) (Jacob et al., 2004; Mann and Schmidt, 2003). Compared to air temperature, LST is more sensitive to the land surface change induced by natural factors (e.g. snow) and/or human activities (e.g. irrigation) (Voogt and Oke, 2003; Winckler et al., 2019). Therefore, LST can be considered to be a good indicator of climate change, and has the potential to provide a new insight into our understanding of the effect of irrigation on the land surface.

The lack of previous research into the effect of irrigation on LST can be largely attributed to the difficulty of acquiring enough surface temperature observations by the traditional methods (i.e. meteorological stations and field experiments). In recent years, with the development of remote sensing techniques, LST data can now be easily obtained from satellites. The high-quality and spatially continuous satellite LST data, such as the Moderate Resolution Imaging Spectroradiometer (MODIS) products, have been widely applied in environmental and climate research, including the assessment of irrigation effects (Balsamo et al., 2018; Tomlinson et al., 2011; Zhou et al., 2018). For instance, regional studies based on satellite LST data found an obvious ICE in Jilin province, China (Zhu et al., 2011), and Indian river basins (Shah et al., 2019), and the capability of satellite LST data in evaluating the climatic effects of irrigation was revealed in another regional study using both meteorological observations and MODIS LST datasets (Zhu et al., 2012).

However, compared with previous research based on near-surface air temperature, studies focusing on the effect of irrigation on LST using satellite observations are still scarce, and most of them are limited to relatively small regions.

In this paper, we propose an ICE detection (ICED) method to quantify the effect of irrigation on LST across China using multi-source remote sensing data. This method can adapt the size of the remote sensing window to the local topographic conditions, and can assess the LST difference between irrigated and adjacent non-irrigated areas. The objective of this study was to present a quantitative assessment of the spatiotemporal patterns of the effect of irrigation on LST in China.

## **2. Study area and datasets**

### **2.1. Study area**

China has always faced food security challenges because of the asymmetry between population and arable land (Zhang, 2011). As an effective way to improve crop yield, irrigation has been paid a lot attentions (Huang et al., 2006). The irrigated area in China has increased dramatically in recent decades. At present, the total irrigated area in China is 61.7 million ha, which accounts for about 50% of the total cropland, which in turn contributes more than 75% of the national food production (Zhu et al., 2013). The irrigated area in China not only covers

a large area, but is also widely distributed in different climate zones, including arid, semi-arid/humid, and humid (Fig. 1). Moreover, China experiences obvious seasonal dynamics with its monsoon climate. Therefore, China is an ideal study area to assess the spatiotemporal patterns of the effect of irrigation on LST.

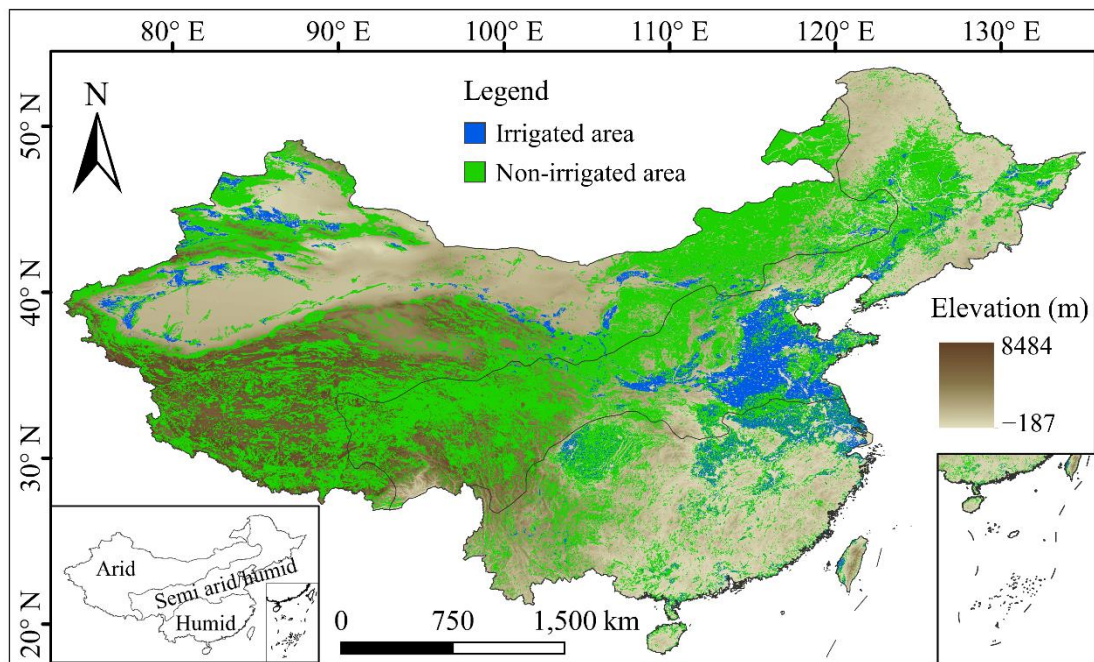


**Fig. 1.** Spatial distribution of the irrigated and non-irrigated areas in China, with the background map indicating the topography. According to the annual average precipitation, we divided China into three climate zones: arid (<400 mm/year), semi-arid/humid (400–800 mm/year), and humid (>800 mm/year). The precipitation map was provided by the Chinese Resource and Environment Data Cloud Platform (<http://www.resdc.cn/>).

## 2.2. Datasets

The surface temperature data for China were obtained from the MODIS LST products. The MODIS LST products have the advantages of

easy access, wide coverage, and high accuracy (Rigo et al., 2006; Wan, 2008; Wan, 2014). In this study, we used the version 6 MODIS LST products from the Terra satellite (MOD11A1) and the Aqua satellite (MYD11A1). These LST data were obtained from 2003 (the year when both types of LST data became available) to 2012 (according to the period of the irrigation product). The retrieval of these MODIS data was further improved by correcting the noise due to cloud contamination, topographic differences, and zenith angle changes (Wan, 2014). Both the MOD11A1 and MYD11A1 products are daily LST products with a spatial resolution of 1 km. Furthermore, these LST data include both daytime (local solar time ~10:30 from Terra and ~13:30 from Aqua) and nighttime (~22:30 from Terra and ~1:30 from Aqua) temperature observations, which allows us to investigate the diurnal (day and night) differences of the ICE.

The delineation of the irrigated and non-irrigated areas was based on the irrigation map provided by Meier et al. (2018) and China's land use/cover datasets (CLUDs) provided by the Chinese Academy of Sciences. Meier's irrigation map was produced by a multiple decision tree architecture, with the integration of multi-temporal NDVI SPOT-VGT data and agricultural suitability data for the period from 1999 to 2012. These data have been validated at both global and regional scales, and have been used in a number of studies (Puy, 2018; Wine, 2019). We

selected this irrigation map because it reflects the actual irrigated area with a higher spatial resolution (30 arc-seconds, ~1 km) than other popular irrigation maps, such as GMIA and MIRCA2000 (5 arc-minutes). In fact, the temperature difference can be caused by both irrigation and land-cover difference. However, the irrigation map does not include land-cover information. To overcome this problem, a land-cover map derived from the CLUDs was applied in this study. The CLUDs have been used in various studies (Huang et al., 2019; Huang et al., 2017; Yang et al., 2017; Yao et al., 2017) for their high resolution (30 m) and good accuracy (approximately 90%) (Kuang et al., 2016).

Surface water areas (lakes and rivers) were not included in the analysis. The surface water areas were obtained from the global surface water (GSW) map produced by Pekel et al. (2016). The GSW map can provide the maximum water extent over the land surface with a high resolution of 30 m. In addition, the 30-m resolution digital elevation model obtained from the Space Shuttle Radar and Topography Mission (SRTM) was used to reduce the influence of the topographic relief when quantifying the impact of irrigation (see Methods).

### **3. Methods**

#### **3.1. Data processing**

The MODIS LST products were first filtered according to their data

quality control (QC) layers, and the LST data with error  $\geq 1$  K were removed. We then aggregated all the daily LST MODIS data into monthly and annual averages based on the observations from 2003 to 2012. The use of multi-year data was aimed at increasing the amount of available high-quality data and minimizing the influence of interannual climate variability (Li et al., 2015). The processing and downloading of these MODIS data was undertaken on the Google Earth Engine (GEE) platform (Gorelick et al., 2017).

Meier's irrigation map and the land-cover map (CLUDs) were combined to distinguish irrigated and non-irrigated areas. The irrigation map can tell us whether a pixel is irrigated or not, and the land-cover map is able to reflect the pixel's surface type (cropland, grassland, or other classes). In this paper, "irrigated area" refers only to irrigated cropland, due to the dominant position of agriculture in irrigated regions (Zhu et al., 2013). "Non-irrigated area" refers to both non-irrigated cropland and non-irrigated grassland which shares a similar surface temperature to non-irrigated cropland (see Section 5.4). The spatial extent of the irrigated and non-irrigated areas is shown in Fig. 1.

### 3.2. The irrigation cooling effect detection method

In this study, the impacts of irrigation were quantified by comparing the LST differences between irrigated and non-irrigated areas. How to select the irrigated and non-irrigated areas for the comparison is thus the

key point. Firstly, the irrigated and non-irrigated areas should be close in distance and share similar climatic conditions (e.g. precipitation and solar radiation). Secondly, the elevation difference between the irrigated area and non-irrigated area must be controlled over a small range because temperature is sensitive to elevation variation. Lastly, the non-irrigated area around the irrigated area needs to be large enough to represent the background surface temperature.

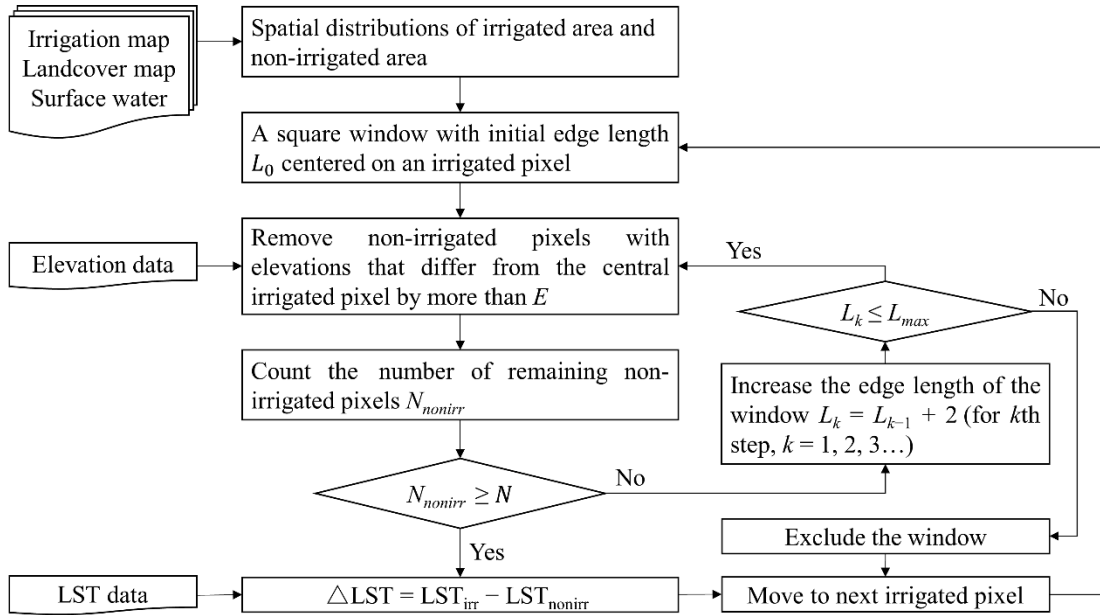


**Fig. 2.** Flowchart of the irrigation cooling effect detection (ICED) method. The default parameter values were set as:  $L_0 = 40$  km,  $N = 10$ ,  $E = 50$  m, and  $L_{max} = 100$  km.

To satisfy the above criteria, we developed an ICE detection method (i.e. the ICED method). The workflow of the proposed ICED method is provided in Fig. 2. The most important part of this method is the dynamic

process of removing the influence of topographic relief. For an irrigated pixel, we search for non-irrigated pixels around it in a square window. The edge length of the square window is increased step by step from the initial value ( $L_0$ ). At each step, the non-irrigated pixels with an elevation out of range ( $E$  meters higher or lower than the elevation of the central irrigated pixel) are removed. This process continues until the number of remaining non-irrigated pixels in the window is larger than a threshold value ( $N$ ). The impact of irrigation on LST can then be quantified using the following equation:

$$\Delta LST = LST_{\text{irr}} - LST_{\text{nonirr}}$$

where  $LST_{\text{irr}}$  is the LST of the central irrigated pixel, and  $LST_{\text{nonirr}}$  is the average LST of the non-irrigated pixels in the square window. A negative (positive)  $\Delta LST$  indicates a cooling (warming) effect. In addition, the edge length of the window must be no greater than the maximum value ( $L_{\text{max}}$ ), otherwise the window is excluded. The values of these parameters for the ICED method in this study were set as:  $L_0 = 40$  km,  $N = 10$ ,  $E = 50$  m, and  $L_{\text{max}} = 100$  km. Sensitivity tests of these parameters are presented in Section 4.3. The ICED method was applied to calculate the  $\Delta LST$  in the window centered at each irrigated pixel across China.

## 4. Results

### 4.1. Diurnal effects of irrigation on LST and their spatial variations

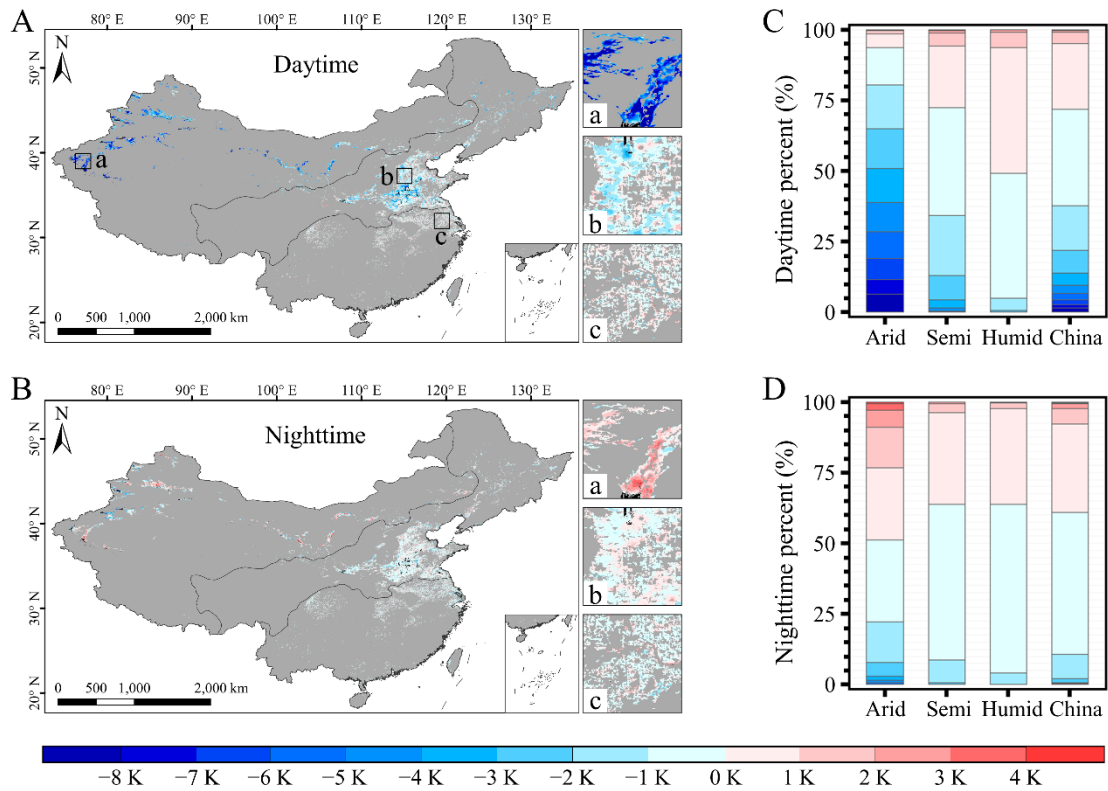


**Fig. 3.** Spatial patterns (A, B) and stacked frequency distributions (C, D) of the annual LST difference ( $\Delta$ LST) between irrigated and non-irrigated areas. The insets (a)–(c) depict the  $\Delta$ LST of three important irrigated districts: (a) Tarim, (b) the North China Plain, and (c) the lower reaches of the Yangtze River. Negative (positive)  $\Delta$ LST indicates a cooling (warming) effect. The gray pixels in (A) and (B) represent the background, and the black pixels represent locations where  $\Delta$ LST could not be calculated (see Methods). Arid, semi, and humid represent the arid climate zone, semi-arid/humid climate zone, and humid climate zone, respectively.

During daytime, irrigation generally has a cooling effect on the land surface. About 72% of the irrigated areas have a lower daytime LST than the non-irrigated areas across China (Fig. 3 C), and the average annual daytime  $\Delta$ LST is  $-1.15 \pm 2.06$  K (mean  $\pm$  SD) at the national scale (Fig. 4A). The most obvious daytime cooling effect can be seen in the arid climate zone, where nearly all the irrigated areas have a cooler surface

than non-irrigated areas (Fig. 3 A, C), and the average  $\Delta\text{LST}$  reaches  $-3.48 \pm 2.40$  K (Fig. 4A). However, in the semi-arid/humid climate zone, although cooling is still the dominant effect in the majority of the irrigated areas relative to non-irrigated areas during daytime (Fig. 3 A, C), the average magnitude of  $\Delta\text{LST}$  is only  $-0.69 \pm 1.23$  K (Fig. 4A). In the humid climate zone, the mean value of annual daytime  $\Delta\text{LST}$  is almost zero (Fig. 4A), indicating the weak impact of irrigation on the land surface in humid regions.

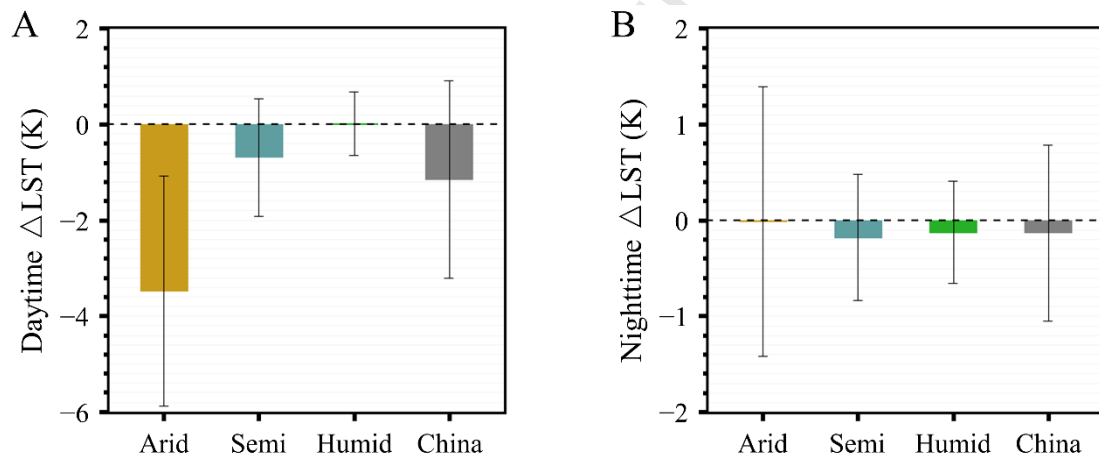


**Fig. 4.** Difference (mean  $\pm$  SD) in annual LST ( $\Delta\text{LST}$ ) between irrigated and non-irrigated areas during (A) daytime and (B) nighttime. Negative (positive)  $\Delta\text{LST}$  indicates a cooling (warming) effect. Arid, semi, and humid represent the arid climate zone, semi-arid/humid climate zone, and humid climate zone, respectively.

During night, the effect of irrigation on LST is generally weaker than during daytime. Most of the nighttime LST differences between irrigated and non-irrigated areas are within  $\pm 1$  K (Fig. 3 B, D), and the average annual nighttime  $\Delta\text{LST}$  is  $-0.13 \pm 0.92$  K across China (Fig. 4 B). The

spatial patterns of  $\Delta LST$  at night are also different from those during daytime. In the arid climate zone, the cooling effect of irrigation is weakened a lot and may even transform into a warming effect at night. Only half of the irrigated areas in the arid climate zone show a lower nighttime LST than the non-irrigated areas (Fig. 3 D), and the annual mean value of the  $\Delta LST$  is around zero at night (Fig. 4 B). In the semi-arid/humid and humid climate zones, irrigation generally has a weak cooling effect on the land surface at night, as indicated by the weak negative averages of the annual nighttime  $\Delta LST$  (Fig. 4 B).

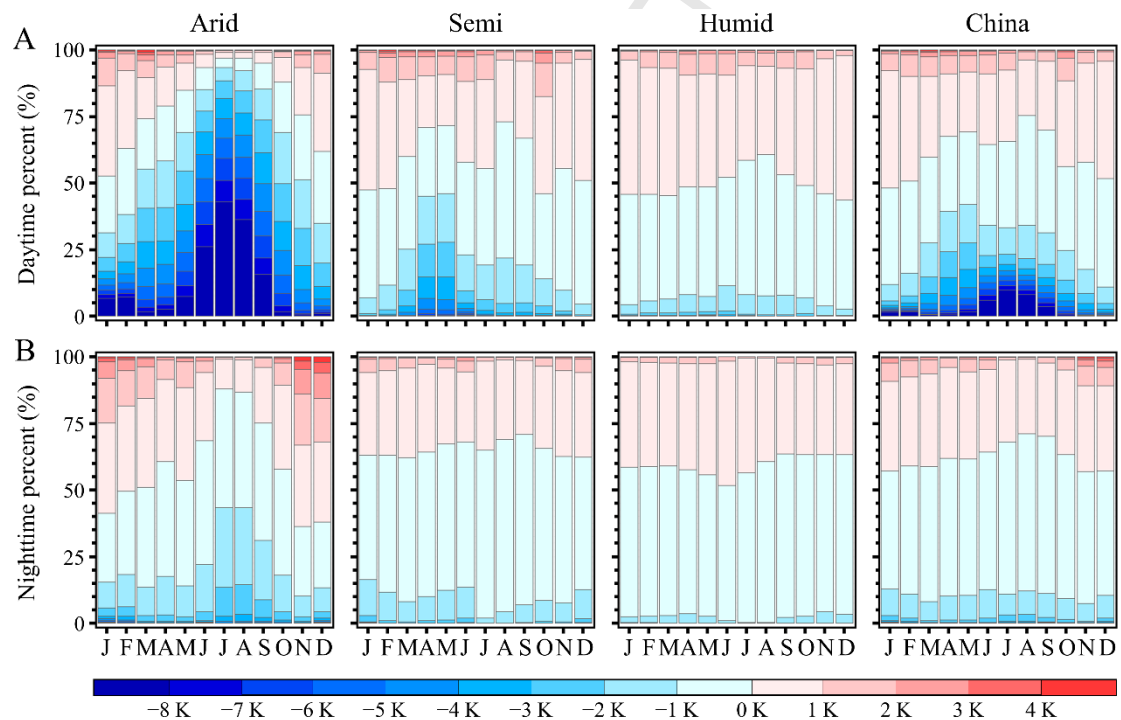


**Fig. 5.** Seasonal variations of the stacked frequency distributions of the (A) daytime and (B) nighttime LST difference ( $\Delta LST$ ) between irrigated and non-irrigated areas. Negative (positive)  $\Delta LST$  indicates a cooling (warming) effect. Arid, semi, and humid represent the arid climate zone, semi-arid/humid climate zone, and humid climate zone, respectively.

#### 4.2. Seasonal effects of irrigation on LST and their spatial patterns

The effect of irrigation on LST shows a clear seasonal variation, which is generally characterized as a stronger cooling effect during the growing season (from May to September) than the non-growing season (Figs. 5–6). At the national scale, the average of daytime  $\Delta$ LST during the growing season ranges from  $-1.76$  K to  $-1.21$  K, which is higher than that during the non-growing season (at mostly less than  $-0.5$  K) (Fig. 6 D1). Similar seasonal patterns also occur in the nighttime (Fig. 6 D2). At night, the national mean  $\Delta$ LST varies from  $-0.33$  K to  $-0.16$  K during the growing season, and is generally around  $-0.1$  K during the non-growing season (Fig. 6 D2).

This seasonality of  $\Delta$ LST shows great spatial heterogeneity, and the most obvious seasonal variation is observed in the arid climate zone. During the growing season, over 90% of the irrigated areas in the arid climate zone show lower daytime LST than the non-irrigated areas (negative  $\Delta$ LST, Fig. 5 A), leading to a substantial cooling effect, with  $\Delta$ LST at more than  $-6$  K (Fig. 6 A1). Meanwhile, in the non-growing season, the average daytime  $\Delta$ LST in the arid climate zone is around  $-1$  K (Fig. 6 A1), because of the relatively small percentage of negative  $\Delta$ LST (mostly less than 65%, Fig. 5 A). A similar seasonality for daytime

$\Delta$ LST is also apparent in the other climate zones, but with a much smaller amplitude of variation (Figs. 5–6). The nighttime  $\Delta$ LST shows an obvious seasonal variation ( $\Delta$ LST in the growing season is much lower than that in the non-growing season) in the arid climate zone (Fig. 6 A2); however, this effect seems to be stable in the different seasons in the semi-arid/humid and humid climate zones (Fig. 6 B2, C2). Overall, irrigation tends to have a more extensive and more intense cooling effect on LST in the arid climate zone during the growing season.

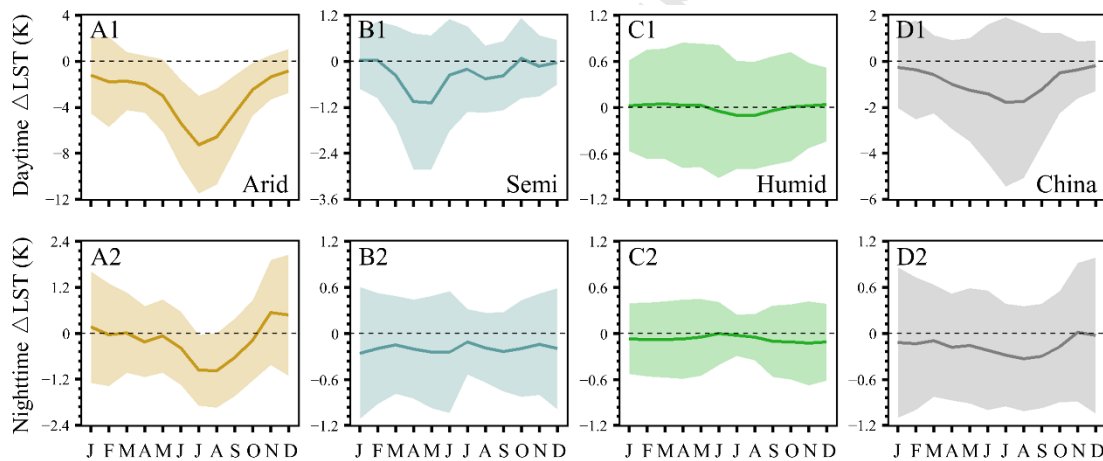


**Fig. 6.** Seasonal variations of the mean and SD (i.e. standard deviation) of the daytime (A1–D1) and nighttime (A2–D2) LST difference ( $\Delta$ LST) between irrigated and non-irrigated areas. Negative (positive)  $\Delta$ LST indicates a cooling (warming) effect. Arid, semi, and humid represent the arid climate zone, semi-arid/humid climate zone, and humid climate zone, respectively.

#### 4.3. Sensitivity tests of the parameters in the ICED method.

The ICED method includes four parameters, namely, the initial edge length of the window ( $L_0$ ), the minimum number of non-irrigated pixels

( $N$ ), the threshold value of elevation ( $E$ ), and the maximum edge length of the window ( $L_{\max}$ ). The sensitivity analysis was applied to study the dependence of the ICE magnitude assessment on these parameters.

We set  $L_0$  to different values (30 km, 50 km, and 60 km) around the default (40 km), and conducted comparison experiments with all the other parameters fixed. We found that the change of  $L_0$  can slightly alter the magnitude of  $\Delta\text{LST}$  in local area, because of the direct impact of  $L_0$  on the size of the search window. However, the influence of  $L_0$  on  $\Delta\text{LST}$  is relatively small, as indicated by the high correlation ( $R > 0.92$ ,  $P < 0.0001$ , Fig. 7) between  $\Delta\text{LST}$  in the comparison experiment ( $L_0 = 30$  km, 50 km, or 60 km) and that in the initial experiment ( $L_0 = 40$  km). Thus, the spatial patterns of  $\Delta\text{LST}$  are consistent with different values of  $L_0$  (Fig. 7).

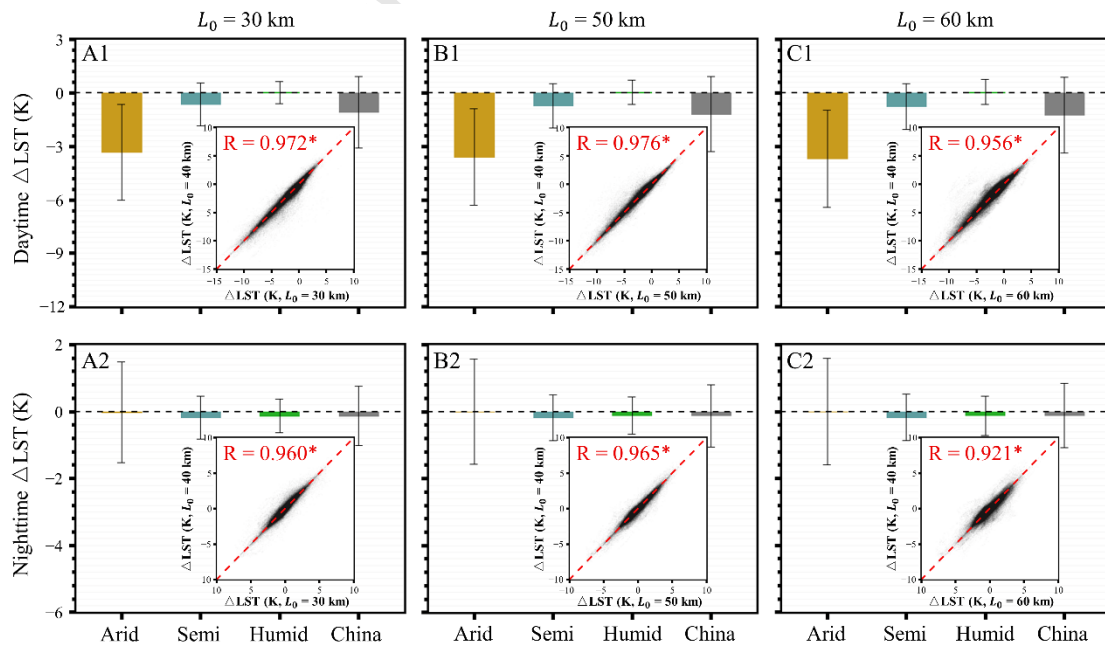


**Fig. 7.** The averages of annual daytime (A1–C1) and nighttime (A2–C2)  $\Delta\text{LST}$ s in the comparison experiments with different values of  $L_0$  (30 km, 50 km, and 60 km).

The insets show the correlation between the  $\Delta$ LST of the comparison experiments and that of the initial experiment ( $L_0 = 40$  km). The red dotted line is the 1:1 line, and the red asterisk indicates that the significance of the correlation is at the 0.0001 level. Arid, semi, and humid represent the arid climate zone, semi-arid/humid climate zone, and humid climate zone, respectively.

We also undertook sensitivity tests of  $N$  (15 and 30, default is 10) and  $E$  (60 m and 100 m, default is 50 m), respectively. A larger value of  $N$  tends to yield a bigger search window, but the identified patterns of  $\Delta$ LST are essentially the same, in view of the strong correlation ( $R > 0.97$ ,  $P < 0.0001$ , Fig. 8 A, B). Similarly, the choice of  $E$  has a negligible influence on the spatial patterns of  $\Delta$ LST ( $R > 0.97$ ,  $P < 0.0001$ , Fig. 8 C, D). The size of the search window should be no more than  $L_{\max}$ , or the search window is excluded. The percentage of excluded search windows across China is very small (0.34–0.75%) when the value of  $L_{\max}$  (80–120 km) is around the default (100 km), which suggests that our results are robust against the choice of  $L_{\max}$ .

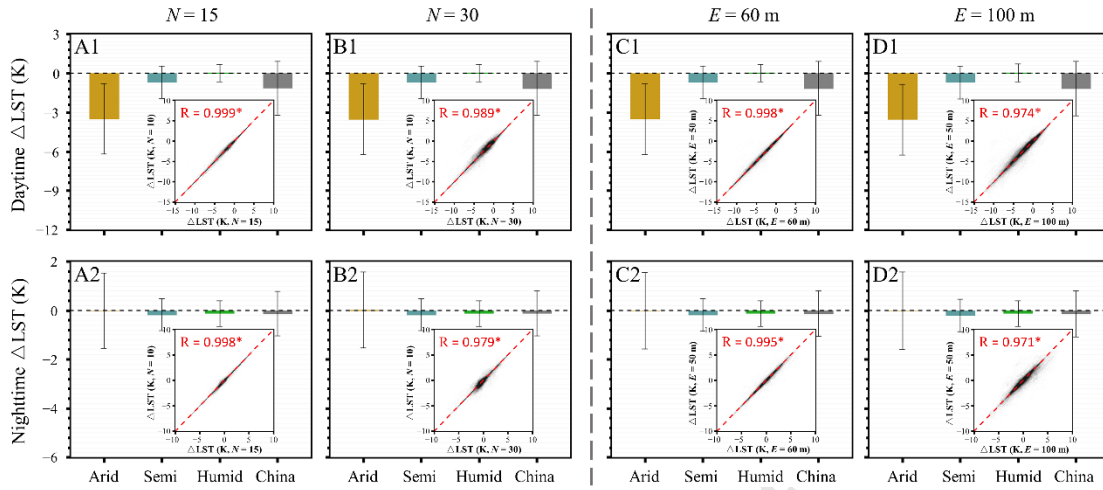


**Fig. 8.** The averages of annual daytime and nighttime  $\Delta$ LSTs in the comparison experiments with different values of  $N$  (15 and 30, A–B) or  $E$  (60 m and 100 m, C–D). The insets show the correlation between the  $\Delta$ LST of the comparison experiments and that of the initial experiment ( $N = 10$  or  $E = 50$  m). The red dotted line is the 1:1 line, and the red asterisk indicates that the significance of the correlation is at the 0.0001 level. Arid, semi, and humid represent the arid climate zone, semi-arid/humid climate zone, and humid climate zone, respectively.

## 5. Discussion

### 5.1. Mechanisms underlying the spatiotemporal variation of the effect of irrigation on LST

The widely observed ICE (i.e. irrigation cooling effect) on LST across China can be mainly attributed to the following reasons. Firstly, irrigation increase soil moisture, which in turn enhances soil evaporation and crop transpiration (i.e. evapotranspiration), and therefore has a direct cooling effect on the land surface because more sensible heat fluxes are repartitioned into latent heat fluxes (Biggs et al., 2008; Cook et al., 2010;

Seneviratne et al., 2010; Zhang et al., 2017). Secondly, the increase of atmospheric water vapor in irrigated areas leads to more cloud cover, which in turn enhances the reflected solar radiation and reduces the total downwelling radiation, having an indirect cooling effect on the land surface (Cook et al., 2014; Qian et al., 2013; Sacks et al., 2009).

The above mechanisms, including changes in evapotranspiration and cloud cover feedback, provide a plausible explanation for the widely observed ICE across China, and their joint effect drives the spatiotemporal variations of the effect of irrigation on LST. For example, the ICE magnitude in the growing season is found to be typically larger than that in the non-growing season (Figs. 5–6). This is because evapotranspiration tends to peak during the growing season, which can result in more transformation of surface net radiation to latent heat fluxes and therefore a substantial cooling effect (Jiang et al., 2014; Wen and Jin, 2012; Zhang et al., 2017). In addition, daytime ICE is generally stronger than that at night (Fig. 4). This can be explained as follows: 1) diurnal asymmetry of the evapotranspiration (high during the day and minimal at night) (Lobell et al., 2008b); and 2) the opposite roles of cloud cover in the land-atmosphere heat fluxes during daytime (reducing downwelling solar radiation) and nighttime (emitting longwave radiation fluxes) (Cook et al., 2014). The ICE is considerable in the arid climate zone, but is negligible in the humid climate zone (Figs. 3–4). This obvious spatial

difference of the impact of irrigation on LST is related to the local background (Lobell et al., 2009; Yu et al., 2018). In the arid climate zone, the additional water provided through irrigation greatly increases the soil moisture, and thus has a great effect on local biophysical processes (e.g. air humidity and evapotranspiration), which leads to the distinct difference in surface temperature between the irrigated and non-irrigated areas. However, in the humid climate zone, the soil moisture is naturally high, and the additional water provided through irrigation has a weaker impact on the land surface than in the arid climate zone. Generally speaking, the spatiotemporal variations of the ICE are closely linked to the changes in surface energy fluxes which are modulated by the mechanisms discussed above. Several other human activities (e.g. fertilization and harvesting) may also play a role in the LST difference between the irrigated and non-irrigated areas. In the future, researchers should make a full-range analysis to further deepen our understanding of the mechanism behind the impact of irrigation on LST.

## 5.2. Implications of the irrigation-induced decrease in LST

LST is recognized as one of the most important parameters in the physics of land surface processes (Li et al., 2013). It plays a central role in the surface energy balance, and modulates the near-surface air temperature through heat flux interaction between land and atmosphere (Jin and Dickinson, 2010; Mildrexler et al., 2011; Shiflett et al., 2017).

The cooling effect of irrigation on LST can be expected to propagate to the atmosphere, and thus induce a decrease in near-surface air temperature. As indicated by previous studies focused on near-surface air temperature, the irrigation-induced cooling effect has been found to largely relieve and even suppress the warming effect caused by greenhouse gas emissions in several arid areas with abundant irrigation (Kueppers et al., 2007; Lobell et al., 2008b). However, it should be noted that human thermal comfort is not only linked with temperature, but is also related to atmospheric humidity (Gaffen and Ross, 1999; Willett et al., 2007). Although irrigation reduces temperature, it also, in parallel, increases atmospheric humidity, which can result in extra heat stress to human bodies when the temperature is high (Li et al., 2018). As revealed by a regional study, irrigation is likely to increase the risk of heatwaves in the North China Plain, due to the high air moisture (Kang and Eltahir, 2018). Therefore, the practical significance of the irrigation-induced decrease in LST is dependent on the local background; for example, irrigation has the potential to counteract the negative impact of global warming in arid regions, but may increase the thermal risk in some humid areas.

Besides thermal comfort, the irrigation-induced decrease in LST might also have an influence on precipitation. Apparently, irrigation can be expected to increase local precipitation because of the positive feedback

between soil moisture and precipitation (Kang and Eltahir, 2019; Moore and Rojstaczer, 2001; Zhang et al., 2017). However, the cooling effect of the irrigation complicates this process. Irrigation can decrease the surface temperature, which enhances the atmospheric stability and induces the downdraft anomaly, resulting in a negative impact on precipitation (Wu et al., 2018; Yang et al., 2016). Thus, not taking the cooling effect of irrigation into account may cause bias or even lead to contrary conclusions when projecting the irrigation-driven climate change.

### 5.3. Uncertainties from the MODIS LST data

The MODIS LST data have been extensively evaluated using in-situ data over China and worldwide (Wan, 2008; Wan, 2014; Wan et al., 2010). These studies have proved the high accuracy of the MODIS LST data for different land covers. For example, Wan (2008) reported that the accuracy of the version 5 MODIS LST data was better than 1 K, and that the root-mean-square error (RMSE) was less than 0.7 K for 47 sites. In this study, we applied the latest version 6 MODIS LST product, whose accuracy has been reported to be better than 0.8 K in 11 sites, with a low RMSE ( $< 0.5$  K) (Wan, 2014). These validation efforts suggest that the MODIS LST data are suitable for the ICE assessment, as they have been widely used for urban heat island assessment (Cao et al., 2016; Peng et al., 2018; Peng et al., 2012; Yang et al., 2019; Zhao et al., 2014).

In addition to accuracy, time period of the MODIS LST data is another

concern. In this study, the MODIS LST data aggregated from 2003 to 2012 were used to assess the effect of irrigation on LST (i.e.  $\Delta$ LST), and changes in the time period of the MODIS LST data may cause uncertainties to our results. To address this issue, we made comparison experiments by comparing the original  $\Delta$ LST (using the MODIS LST data from 2003 to 2012) to the  $\Delta$ LSTs using the MODIS LST data of other time periods (2003-2007 and 2008-2012), and the correlations between them are shown in Fig. 9. The original  $\Delta$ LST is highly ( $R > 0.970$ ) and significantly ( $P < 0.0001$ ) correlated to those using the MODIS LST data of other time periods, which indicates that using the MODIS LST data of different time period is unlikely to influence the identified patterns of  $\Delta$ LST.

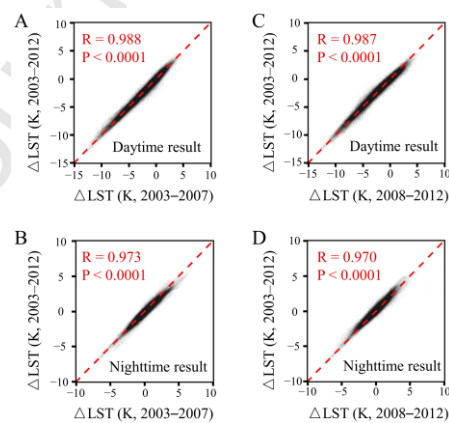


**Fig. 9.** The correlations between the  $\Delta$ LST using the MODIS LST data of the original time period (2003–2012) and those using the MODIS LST data of other time periods (2003–2007 and 2008–2012). The red dotted line is the 1:1 line.

#### 5.4. Limitations of this study

Several limitations in the present study need to be addressed. Firstly, due to the scarcity of non-irrigated cropland in northwestern China (mostly the arid climate zone), we included non-irrigated grassland in the non-irrigated area. This land-cover difference across the non-irrigated area might cause bias to our results. The average LST difference between non-irrigated cropland and non-irrigated grassland in the arid climate zone is about  $-0.25$  K during annual daytime, which is small compared to the detected ICE magnitude (approximately  $-3.50$  K, Fig. 4A). At the national scale, the average annual daytime LST difference between non-irrigated cropland and non-irrigated grassland is about  $-0.10$  K, which is much weaker than the average magnitude of the LST difference between irrigated and non-irrigated areas ( $-1.15$  K, Fig. 4A). These findings indicate that the uncertainty caused by the grassland is acceptable, and it is unlikely to have had a significant influence on the identified spatiotemporal patterns of the ICE. Secondly, our study was based on a static irrigation map, due to the lack of dynamic irrigation maps for China. This limits the study of the impact of irrigation expansion on the spatiotemporal variation of LST.

## 6. Conclusions

In this paper, based on satellite observations, we have proposed the novel ICED method and made a comprehensive quantitative assessment

of the effect of irrigation on LST across China. Irrigation generally has a cooling effect on LST, as indicated by the lower LST in irrigated areas than in adjacent non-irrigated areas across China during daytime (annual average  $\Delta\text{LST} = -1.15 \pm 2.06$  K) and nighttime (annual average  $\Delta\text{LST} = -0.13 \pm 0.92$  K). This irrigation cooling effect (i.e. ICE) shows obvious spatiotemporal heterogeneity across China, which is generally characterized by stronger ICE magnitude in the arid climate zone and in the growing season. The average magnitude of daytime ICE was found to be greater than 6 K in the arid climate zone during the growing season, but was found to be around zero in the humid climate zone throughout the year. Our findings will provide useful information for researchers studying the impact of irrigation on LST and regional climate, and the ICED method has the potential to be applied to other irrigated regions.

### **Acknowledgments**

This research was supported by the National Natural Science Foundation of China under grants 41790424, 41771360, and 41971295; the National Program for Support of Top-notch Young Professionals; the Hubei Provincial Natural Science Foundation of China under grant 2017CFA029; the National Key R&D Program of China under grant 2016YFB0501403; and the Shenzhen Science and Technology Program under grant JCYJ20180306170645080.

## References

- Balsamo G, Agusti-Panareda A, Albergel C, Arduini G, Beljaars A, Bidlot J, et al., 2018. Satellite and In Situ Observations for Advancing Global Earth Surface Modelling: A Review. *Remote Sensing*. 10, 2038.
- Biggs TW, Scott CA, Gaur A, Venot J-P, Chase T, Lee E, 2008. Impacts of irrigation and anthropogenic aerosols on the water balance, heat fluxes, and surface temperature in a river basin. *Water Resour. Res.* 44, W12415.
- Bonfils Cl, Lobell D, 2007. Empirical evidence for a recent slowdown in irrigation-induced cooling. *Proc. Natl. Acad. Sci. U. S. A.* 104, 13582-13587.
- Broadbent AM, Coutts AM, Tapper NJ, Demuzere M, 2018. The cooling effect of irrigation on urban microclimate during heatwave conditions. *Urban Clim.* 23, 309-329.
- Cao C, Lee X, Liu S, Schultz N, Xiao W, Zhang M, et al., 2016. Urban heat islands in China enhanced by haze pollution. *Nat. Commun.* 7, 12509.
- Chen F, Xu X, Barlage M, Rasmussen R, Shen S, Miao S, et al., 2018. Memory of irrigation effects on hydroclimate and its modeling challenge. *Environ. Res. Lett.* 13, 064009.
- Chen X, Jeong S-J, 2018. Irrigation enhances local warming with greater

- nocturnal warming effects than daytime cooling effects. *Environ. Res. Lett.* 13.
- Chou C, Ryu D, Lo M-H, Wey H-W, Malano HM, 2018. Irrigation-Induced Land–Atmosphere Feedbacks and Their Impacts on Indian Summer Monsoon. *J. Clim.* 31, 8785-8801.
- Cook BI, Puma MJ, Krakauer NY, 2010. Irrigation induced surface cooling in the context of modern and increased greenhouse gas forcing. *Clim. Dyn.* 37, 1587-1600.
- Cook BI, Shukla SP, Puma MJ, Nazarenko LS, 2014. Irrigation as an historical climate forcing. *Clim. Dyn.* 44, 1715-1730.
- de Vrese P, Hagemann S, 2017. Uncertainties in modelling the climate impact of irrigation. *Clim. Dyn.* 1-16.
- Gaffen DJ, Ross RJ, 1999. Climatology and Trends of U.S. Surface Humidity and Temperature. *J. Clim.* 12, 811-828.
- Godfray HCJ, Beddington JR, Crute IR, Haddad L, Lawrence D, Muir JF, et al., 2010. Food security: the challenge of feeding 9 billion people. *Science.* 327, 812–818.
- Goonetilleke A, Thomas E, Ginn S, Gilbert D, 2005. Understanding the role of land use in urban stormwater quality management. *J. Environ. Manag.* 74, 31-42.
- Gorelick N, Hancher M, Dixon M, Ilyushchenko S, Thau D, Moore R, 2017. Google Earth Engine: Planetary-scale geospatial analysis for

- everyone. *Remote Sens. Environ.* 202, 18-27.
- Grimm NB, Faeth SH, Golubiewski NE, Redman CL, Wu J, Bai X, et al., 2008. Global Change and the Ecology of Cities. *Science*. 319, 756-760.
- Han S, Yang Z, 2013. Cooling effect of agricultural irrigation over Xinjiang, Northwest China from 1959 to 2006. *Environ. Res. Lett.* 8, 024039.
- Huang Q, Rozelle S, Lohmar B, Huang J, Wang J, 2006. Irrigation, agricultural performance and poverty reduction in China. *Food Policy*. 31, 30-52.
- Huang X, Cai Y, Li J, 2019. Evidence of the mitigated urban particulate matter island (UPI) effect in China during 2000-2015. *Sci. Total Environ.* 660, 1327-1337.
- Huang X, Xia J, Xiao R, He T, 2017. Urban expansion patterns of 291 Chinese cities, 1990–2015. *Int. J. Digit. Earth*. 12, 62-77.
- Jacob F, Petitcolin Fo, Schmugge T, Vermote E, French A, Ogawa K, 2004. Comparison of land surface emissivity and radiometric temperature derived from MODIS and ASTER sensors. *Remote Sens. Environ.* 90, 137-152.
- Jiang L, Ma E, Deng X, 2014. Impacts of Irrigation on the Heat Fluxes and Near-Surface Temperature in an Inland Irrigation Area of Northern China. *Energies*. 7, 1300-1317.

- Jin M, Dickinson RE, 2010. Land surface skin temperature climatology: Benefitting from the strengths of satellite observations. *Environ. Res. Lett.* 5, 1748-9326.
- Kang S, Eltahir EAB, 2018. North China Plain threatened by deadly heatwaves due to climate change and irrigation. *Nat. Commun.* 9, 2894.
- Kang S, Eltahir EAB, 2019. Impact of Irrigation on Regional Climate Over Eastern China. *Geophys. Res. Lett.* 46, 5499-5505.
- King MD, 1999. EOS science plan: the state of science in the EOS program: National Aeronautics and Space Administration.
- Kuang W, Liu J, Dong J, Chi W, Zhang C, 2016. The rapid and massive urban and industrial land expansions in China between 1990 and 2010: A CLUD-based analysis of their trajectories, patterns, and drivers. *Landsc. Urban Plann.* 145, 21-33.
- Kueppers LM, Snyder MA, Sloan LC, 2007. Irrigation cooling effect: Regional climate forcing by land-use change. *Geophys. Res. Lett.* 34, L03703.
- Li J, Chen YD, Gan TY, Lau N-C, 2018. Elevated increases in human-perceived temperature under climate warming. *Nat. Clim. Change.* 8, 43-47.
- Li Y, Zhao M, Motesharrei S, Mu Q, Kalnay E, Li S, 2015. Local cooling and warming effects of forests based on satellite observations. *Nat.*

- Commun. 6, 6603.
- Li Z-L, Tang B-H, Wu H, Ren H, Yan G, Wan Z, et al., 2013. Satellite-derived land surface temperature: Current status and perspectives. *Remote Sens. Environ.* 131, 14-37.
- Lobell D, Bala G, Mirin A, Phillips T, Maxwell R, Rotman D, 2009. Regional differences in the influence of irrigation on climate. *J. Clim.* 22, 2248-2255.
- Lobell DB, Bonfils C, 2008. The effect of irrigation on regional temperatures: a spatial and temporal analysis of trends in California, 1934–2002. *J. Clim.* 21, 2063-2071.
- Lobell DB, Bonfils C, Faurès J-M, 2008a. The Role of Irrigation Expansion in Past and Future Temperature Trends. *Earth Interact.* 12, 1-11.
- Lobell DB, Bonfils CJ, Kueppers LM, Snyder MA, 2008b. Irrigation cooling effect on temperature and heat index extremes. *Geophys. Res. Lett.* 35.
- Mahmood R, Foster S, Keeling T, Hubbard K, Carlson C, Leeper R, 2006. Impacts of irrigation on 20th century temperature in the northern Great Plains. *Glob. Planet. Change.* 54, 1-18.
- Mann ME, Schmidt GA, 2003. Ground vs. surface air temperature trends: Implications for borehole surface temperature reconstructions. *Geophys. Res. Lett.* 30.

- Meier J, Zabel F, Mauser W, 2018. A global approach to estimate irrigated areas - a comparison between different data and statistics. *Hydrol. Earth Syst. Sci.* 22, 1119-1133.
- Mildrexler DJ, Zhao M, Running SW, 2011. A global comparison between station air temperatures and MODIS land surface temperatures reveals the cooling role of forests. *J. Geophys. Res.* 116.
- Moore N, Rojstaczer S, 2001. Irrigation-Induced Rainfall and the Great Plains. *J. Appl. Meteorol.* 40, 1297-1309.
- Nocco MA, Smail RA, Kucharik CJ, 2019. Observation of irrigation- induced climate change in the Midwest United States. *Glob. Change Biol.* 25, 3472-3484.
- Ozdogan M, 2011. Exploring the potential contribution of irrigation to global agricultural primary productivity. *Global Biogeochem. Cycles.* 25, GB3016.
- Pekel J-F, Cottam A, Gorelick N, Belward AS, 2016. High-resolution mapping of global surface water and its long-term changes. *Nature.* 540, 1476-4687.
- Peng J, Ma J, Liu Q, Liu Y, Li Y, Yue Y, 2018. Spatial-temporal change of land surface temperature across 285 cities in China: An urban-rural contrast perspective. *Sci. Total Environ.* 635, 487-497.
- Peng S, Piao S, Ciais P, Friedlingstein P, Oettle C, Breon FM, et al., 2012.

- Surface urban heat island across 419 global big cities. *Environ. Sci. Technol.* 46, 696-703.
- Puy A, 2018. Irrigated areas grow faster than the population. *Ecol. Appl.* 28, 1413-1419.
- Qian Y, Huang M, Yang B, Berg LK, 2013. A Modeling Study of Irrigation Effects on Surface Fluxes and Land–Air–Cloud Interactions in the Southern Great Plains. *J. Hydrometeorol.* 14, 700-721.
- Rigo G, Parlow E, Oesch D, 2006. Validation of satellite observed thermal emission with in-situ measurements over an urban surface. *Remote Sens. Environ.* 104, 201-210.
- Roy SS, Mahmood R, Niyogi D, Lei M, Foster SA, Hubbard KG, et al., 2007. Impacts of the agricultural Green Revolution–induced land use changes on air temperatures in India. *J. Geophys. Res.* 112.
- Sacks WJ, Cook BI, Buening N, Levis S, Helkowski JH, 2009. Effects of global irrigation on the near-surface climate. *Clim. Dyn.* 33, 159-175.
- Seneviratne SI, Corti T, Davin EL, Hirschi M, Jaeger EB, Lehner I, et al., 2010. Investigating soil moisture–climate interactions in a changing climate: A review. *Earth-Sci. Rev.* 99, 125-161.
- Shah HL, Zhou T, Huang M, Mishra V, 2019. Strong Influence of Irrigation on Water Budget and Land Surface Temperature in Indian

- Subcontinental River Basins. *J. Geophys. Res. Atmos.* 124, 1449-1462.
- Shi W, Tao F, Liu J, 2014. Regional temperature change over the Huang-Huai-Hai Plain of China: the roles of irrigation versus urbanization. *Int. J. Climatol.* 34, 1181-1195.
- Shiflett SA, Liang LL, Crum SM, Feyisa GL, Wang J, Jenerette GD, 2017. Variation in the urban vegetation, surface temperature, air temperature nexus. *Sci. Total Environ.* 579, 495-505.
- Thiery W, Davin EL, Lawrence DM, Hirsch AL, Hauser M, Seneviratne SI, 2017. Present-day irrigation mitigates heat extremes. *J. Geophys. Res. Atmos.* 122, 1403-1422.
- Tomlinson CJ, Chapman L, Thornes JE, Baker C, 2011. Remote sensing land surface temperature for meteorology and climatology: a review. *Meteorol. Appl.* 18, 296-306.
- Voogt JA, Oke TR, 2003. Thermal remote sensing of urban climates. *Remote Sens. Environ.* 86, 370-384.
- Wan Z, 2008. New refinements and validation of the MODIS Land-Surface Temperature/Emissivity products. *Remote Sens. Environ.* 112, 59-74.
- Wan Z, 2014. New refinements and validation of the collection-6 MODIS land-surface temperature/emissivity product. *Remote Sens. Environ.* 140, 36-45.

- Wan Z, Zhang Y, Zhang Q, Li ZL, 2010. Quality assessment and validation of the MODIS global land surface temperature. *Int. J. Remote Sens.* 25, 261-274.
- Wen L, Jin J, 2012. Modelling and analysis of the impact of irrigation on local arid climate over northwest China. *Hydrol. Process.* 26, 445-453.
- Willett KM, Gillett NP, Jones PD, Thorne PW, 2007. Attribution of observed surface humidity changes to human influence. *Nature.* 449, 710-2.
- Winckler J, Reick CH, Luysaert S, Cescatti A, Stoy PC, Lejeune Q, et al., 2019. Different response of surface temperature and air temperature to deforestation in climate models. *Earth Syst. Dyn.* 10, 473-484.
- Wine ML, 2019. Under non-stationarity securitization contributes to uncertainty and Tragedy of the Commons. *J. Hydrol.* 568, 716-721.
- Wu L, Feng J, Miao W, 2018. Simulating the impacts of irrigation and dynamic vegetation over the North China Plain on regional climate. *J. Geophys. Res. Atmos.*
- Yang B, Zhang Y, Qian Y, Tang J, Liu D, 2016. Climatic effects of irrigation over the Huang- Huai- Hai Plain in China simulated by the weather research and forecasting model. *J. Geophys. Res. Atmos.* 121, 2246-2264.
- Yang Q, Huang X, Li J, 2017. Assessing the relationship between surface

- urban heat islands and landscape patterns across climatic zones in China. *Sci. Rep.* 7, 9337-9347.
- Yang Q, Huang X, Tang Q, 2019. The footprint of urban heat island effect in 302 Chinese cities: Temporal trends and associated factors. *Sci. Total Environ.* 655, 652-662.
- Yao R, Wang L, Huang X, Niu Z, Liu F, Wang Q, 2017. Temporal trends of surface urban heat islands and associated determinants in major Chinese cities. *Sci. Total Environ.* 609, 742-754.
- Yu Z, Xu S, Zhang Y, Jørgensen G, Vejre H, 2018. Strong contributions of local background climate to the cooling effect of urban green vegetation. *Sci. Rep.* 8.
- Zhang J, 2011. China's success in increasing per capita food production. *J. Exp. Bot.* 62, 3707-11.
- Zhang X, Xiong Z, Tang Q, 2017. Modeled effects of irrigation on surface climate in the Heihe River Basin, Northwest China. *J. Geophys. Res. Atmos.* 122, 7881-7895.
- Zhao L, Lee X, Smith RB, Oleson K, 2014. Strong contributions of local background climate to urban heat islands. *Nature.* 511, 216-219.
- Zhou D, Xiao J, Bonafoni S, Berger C, Deilami K, Zhou Y, et al., 2018. Satellite Remote Sensing of Surface Urban Heat Islands: Progress, Challenges, and Perspectives. *Remote Sens.* 11, 48.
- Zhu X, Li Y, Li M, Pan Y, Shi P, 2013. Agricultural irrigation in China. *J.*

Soil Water Conserv. 68, 147A-154A.

Zhu X, Liang S, Pan Y, 2012. Observational evidence of the cooling effect of agricultural irrigation in Jilin, China. *Clim. Change.* 114, 799-811.

Zhu X, Liang S, Pan Y, Zhang X, 2011. Agricultural Irrigation Impacts on Land Surface Characteristics Detected From Satellite Data Products in Jilin Province, China. *IEEE J. Sel. Topics Appl. Earth Observ. Remote Sens.* 4, 721-729.

Journal Pre-proof

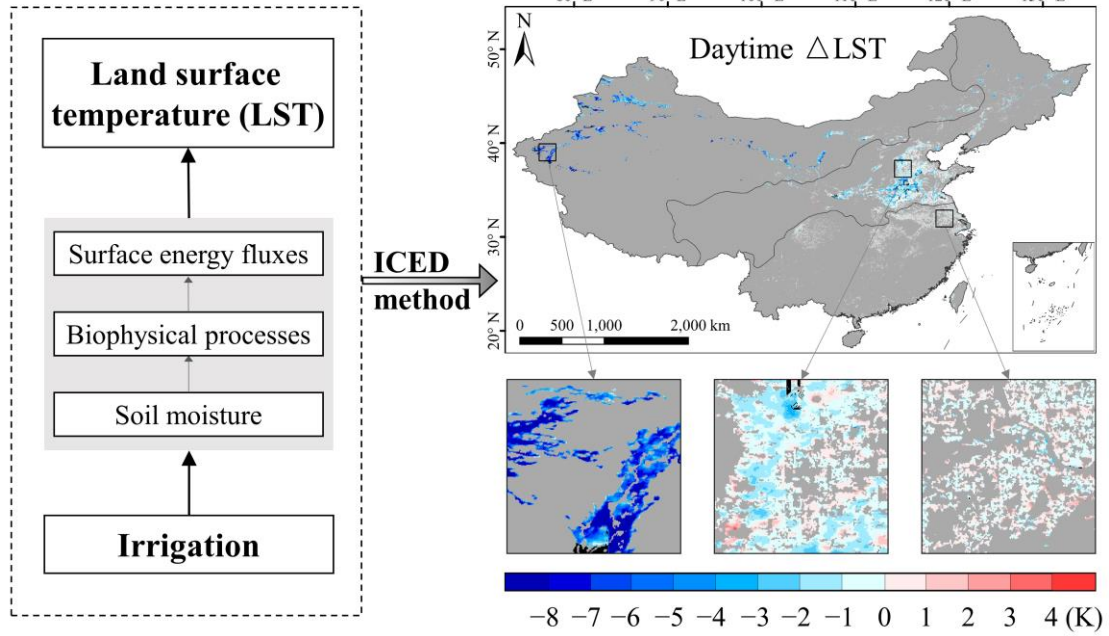
**Declaration of interests**

The authors declare that they have no known competing financial interests or personal relationships that could have appeared to influence the work reported in this paper.

Journal Pre-proof

## Graphical Abstract

Irrigation cooling effect (ICE) on land surface temperature (LST) based on the novel ICE detection (ICED) method



### **Research Highlights**

A novel method is proposed to quantify the effect of irrigation on land surface temperature.

Irrigation averagely decreases daytime land surface temperature by 1.15 K across irrigated areas in China.

The irrigation-induced cooling effect reaches greater than 6 K in the arid area during growing season.

The impact of irrigation on land surface temperature is minor in the humid area.

Journal Pre-proof